Biomedicine & Pharmacotherapy 155 (2022) 113837

Contents lists available at ScienceDirect

Biomedicine & Pharmacotherapy

journal homepage: www.elsevier.com/locate/biopha

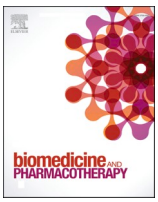

Lipid-polymer nanocarrier platform enables X-ray induced photodynamic therapy against human colorectal cancer cells

Rui Sang [a], Fei Deng [a], Alexander Engel [c,d], Ewa Goldys [a], Wei Deng [b,*]

[a] Graduate School of Biomedical Engineering, ARC Centre of Excellence in Nanoscale Biophotonics, Faculty of Engineering, UNSW Sydney, NSW 2052, Australia
[b] School of Biomedical Engineering, University of Technology Sydney, Sydney, NSW 2007, Australia
[c] Sydney Medical School, University of Sydney, Sydney, NSW 2050, Australia
[d] Department of Colorectal Surgery, Royal North Shore Hospital, St Leonards, NSW 2065, Australia

ARTICLE INFO

Key words:
X-PDT
Targeted lipid-polymer nanoparticles
Verteporfin
5-FU
Colorectal cancer

ABSTRACT

In this study, we brought together X-ray induced photodynamic therapy (X-PDT) and chemo-drug (5-FU) for the treatment on colorectal cancer cells. This was achieved by developing a lipid-polymer hybrid nanoparticle delivery system (FA-LPNPs-VP-5-FU). It was prepared by incorporating a photosensitizer (verteporfin), chemotherapy drug (5-FU) and a targeting moiety (folic acid) into one platform. The average size of these nanoparticles was around 100 nm with low polydispersity. When exposed to clinical doses of 4 Gy X-ray radiation, FA-LPNPs-VP-5-FU generated sufficient amounts of reactive oxygen species, triggering the apoptosis and necrosis pathway of cancer cells. Our combined X-PDT and chemo-drug strategy was effective in inhibiting cancer cells' growth and proliferation. Cell cycle analyses revealed that our treatment induced G2/M and S phase arrest in HCT116 cells. Our results indicate that this combined treatment provides better antitumour effect in colorectal cancer cells than each of these modalities alone. This may offer a novel approach for effective colorectal cancer treatment with reduced off-target effect and drug toxicity.

1. Introduction

Colorectal cancer (CRC) is the second most deadly cancer worldwide [1]. The 5-year survival rate for stage III and stage IV patients are about 65% and 12.5% only [2,3]. In the clinical setting surgical resection is often combined with chemotherapy for colon cancer and with chemo-radiotherapy for patients with rectal cancer. The latter treatments can be given in a neo-adjuvant or adjuvant setting. However, drug resistance, cardiotoxicity and myelosuppression caused by chemotherapy and progressive late morbidity induced by high dose X-ray radiation leads to unsatisfactory therapeutic outcomes for CRC patients, representing inevitable limitations of these treatments [4–6]. Therefore, an effective and safe treatment strategy is highly desired.

Photodynamic therapy (PDT) is an effective treatment approach for superficial cancers. It acts through activating photosensitisers (also known as PDT drug) by near infrared or visible light to generate reactive oxygen species (ROS), which induces cell death via the mechanisms of necrosis, apoptosis and autophagy [7,8]. However, the penetration depth of light used for PDT is limited (no more than 10 mm) due to light absorption by tissues, leading to ineffective activation of photosensitisers and decreased efficacy of PDT for deep seated tumours, including CRC [9]. To overcome the challenges of light-related limited tissue penetration, X-PDT has been proposed by taking advantage of excellent tissue penetrating capability of clinical X-rays [10]. We previously developed a poly lactic-co-glycolic acid (PLGA) nanocarrier platform loaded with photosensitizer verteporfin (VP) or co-loaded with gold nanoparticles for X-PDT on CRC and pancreatic cancer, and efficient cytotoxicity in cancer cells was observed [11–13]. In these studies, VP was directly activated by X-ray irradiation and generated reactive oxygen species (ROS) under different radiation dose for cancer cell killing, not only acted as a clinically approved photosensitiser for PDT in age-related macular degeneration [14]. Moreover, another polymer nanocarriers was developed by using a cationic polymer (poly (allylamine hydrochloride), PAH) to assemble photosensitizer (Rose Bengal) conjugated with Au clusters (radiosensitizers). The nanoparticles exhibited significant therapeutic efficacy for breast cancer through X-PDT [15]. However, to our best of knowledge, few research was reported on the synergistic effect of combined X-PDT and chemo-drugs in CRC cells.

5-Fluorouracil (5-FU) is a frequently used first line chemotherapeutic

* Corresponding author.
E-mail address: Wei.Deng@uts.edu.au (W. Deng).

https://doi.org/10.1016/j.biopha.2022.113837
Received 9 August 2022; Received in revised form 26 September 2022; Accepted 6 October 2022
Available online 9 October 2022

agent for CRC treatment, which works by disrupting DNA and RNA synthesis to trigger CRC cells apoptosis, through a mechanism involving folate metabolism [16]. In addition, 5-FU could be used as a radiosensitizer during chemoradiotherapy [17–19]. In this work we developed lipid-polymer nanocarriers by co-loading VP and 5-FU within a single platform to investigate the potential synergistic effect under X-ray radiation. This nanocarrier was further modified with folic acid to achieve cancer targeting capability, since folic acid has high affinity for folate receptors which are overexpressed on the surfaces of human CRC cells, such as HCT116, compared with healthy cells [20]. The intracellular singlet oxygen ($^1O_2$) generation was further assessed by using Singlet Oxygen Green Sensor (SOSG). Following these studies, we evaluated the anti-cancer effect of our nanoparticle delivery system in combination with low dose of X-ray radiation (4 Gy) in HCT116 cells, by checking cells' viability, cellular apoptosis/necrosis pathway and cell population in the different phases of the cell cycle.

2. Materials and methods

2.1. Materials and chemicals

Lecithin (P7443–100MG) and 1,2-distearoyl-snglycero-3-phosphoethanolamine-N-carboxy (polyethylene glycol) 2000 (DSPE-PEG) (880135 P-100MG) were purchased from Avanti Polar Lipids (Alabaster, USA). 1,2-distearoyl-snglycero-3-phosphoethanolamine-N-carboxy (polyethylene glycol) 2000)-folic acid (DSPE-PEG-folic acid) (PG2-DSFA-2k) was purchased from Nanocs (New York, USA). PLGA (719900–5 G), VP (SML0534–25MG), Chloroform (C2432–500 mL), Acetonitrile (271004–1 L), 2′7′-dichlorofluorescin diacetate (DCF-DA, D6883), McCoy's 5 A Medium (M8403–500 mL) and Pur-A-Lyzer™ Maxi Dialysis Kit (MWCO 12–14 kDa, PURX12015–1KT) were purchased from Sigma-Aldrich Pty Ltd (Sydney, Australia). 5-FU (F6627–1 G) and Amicon Ultra-0.5 Centrifugal Filter Unit (UFC510024) were purchased from Merck Pty Ltd (Melbourne, Australia). SOSG (S36002), MES (0.5 M buffer, pH 7.5, pH 6.0 and pH 5.0), Opti-Minimal Essential Medium (Opti-MEM; reduced serum medium; product, 31985062) and ReadyProbes® Cell Viability Imaging Kit, Blue/Green (R37609) were purchased from Thermo Fisher Scientific Aust Pty Ltd (Sydney, Australia). HCT116 human colon cancer cell line (ATCCCL247) and CCD841 CoN human colon normal cell line (ATCCRL1790) were purchased from ATCC (Manassas, USA). CellTiter 96® AQueous One Solution Cell Proliferation Assay (MTS kit, G3580) was purchased from Promega (Madison, USA). Apoptosis/Necrosis Assay Kits (blue, red, green) (ab176750) was purchased from Abcam (Cambridge, UK). The Luminex Muse® Cell Cycle Kit (LUMCH100106) was purchased from Abacus dx (Brisbane, Australia).

2.2. Methods

2.2.1. Preparation of the lipid-polymer hybrid nanoparticles

Lipid-polymer hybrid nanoparticles were prepared by self-assembly through a single-step nanoprecipitation method [21,22]. Briefly, lecithin/DSPE-PEG (molar ratio, 8.5:1.5, in chloroform) or lecithin/DSPE-PEG/DSPE-PEG-folic acid (for targeting purpose, 8.5:1.0:0.5, in chloroform) was mixed with 9 mL ethanol aqueous solution (4 wt%), followed by heating to 65 °C to uniformly dissolve all lipids in liquid phase. Subsequently, the acetonitrile solution containing PLGA (5 mg/mL), VP (39.75 μM) and 5-FU (1 mg/mL) was dropped into the preheated lipid solution under gentle stirring, with 15% mass ratio of lipid/polymer. This mixture was gently stirred for 2 h at room temperature. The purification of nanoparticles was performed through Pur-A-Lyzer Maxi Dialysis Kit (12–14 kDa) overnight. The prepared nanoparticles were stored at 4 °C for future use.

We prepared several types of lipid-polymer hybrid nanoparticles samples, including folic acid modified nanoparticles encapsulated VP and 5-FU (FA-LPNPs-VP-5-FU), VP and 5-FU co-loaded nanoparticles (LPNPs-VP-5-FU), nanoparticles encapsulated VP or 5-FU only (LPNPs-VP and LPNPs-5-FU) and pure nanoparticles (LPNPs). Their formulations were listed in Table 1:

Table 1
Formulations of prepared lipid-polymer hybrid nanoparticles.

Samples	PLGA (mg/mL)	lecithin/DSPE-PEG/DSPE-PEG-folic acid	VP (μM)	5-FU (mg/mL)
LPNPs	5	8.5:1.5:0	0	0
LPNPs-VP	5	8.5:1.5:0	39.75	0
LPNPs-5-FU	5	8.5:1.5:0	0	1
LPNPs-VP-5-FU	5	8.5:1.5:0	39.75	1
FA-LPNPs-VP-5-FU	5	8.5:1.0:0.5	39.75	1

2.2.2. Characterisation of lipid nanoparticles

The size distribution and zeta potential of prepared nanoparticles were measured using a Zetasizer Nano-ZS (Malvern Panalytical Co., Malvern, UK). The fluorescence spectrum of VP from the nanoparticles was measured using a spectrofluorometer (FluoroMax-4, Horiba Scientific Co., Kyoto, Japan). The absorption spectra of folic acid, 5-FU and folic acid-modified nanoparticles were determined using a spectrophotometer (Cary 5000 UV-Vis-NIR, Agilent Technologies, California, USA). The nanoparticle morphology was carried out by using Transmission Electron Microscopy (TEM) imaging system (JEOL 1400 Transmission Electron Microscope, JEOL Pty. Ltd, Tokyo, Japan). The encapsulation efficiency (EE%) was calculated according to the following equation:

$$EE\% = \text{Drug}_{\text{encapsulated}}/\text{Drug}_{\text{total}} \times 100\%$$

The amounts of VP and 5-FU entrapped in nanoparticles were obtained by measuring the fluorescence intensity of VP (Ex/Em: 425 nm/690 nm) and absorbance of 5-FU at 266 nm after complete dissolution of nanoparticles in acetonitrile and calculating its concentration from the standard curve of free VP and 5-FU solution.

2.2.3. Serum and pH stability studies

200 μL nanoparticle samples were diluted in cell medium (McCoy's 5 A) with or without foetal bovine serum (FBS). All samples were placed in a dialysis device (D-Tube Dialyzer Maxi, 71510, Merck KGaA, Darmstadt, Germany). Subsequently, these devices were kept in 50 mL centrifuge tubes containing 10 mL cell medium at room temperature under continuous gentle shaking. The fluorescence intensity of VP leaked from the nanoparticles into the surrounding solution was measured using a fluorescence spectrometer (FluoroMax, Horiba Scientific, Kyoto, Japan) at various time points (1 h, 4 h, 7 h, 24 h, 48 h, 72 h, 96 h). After 96 h, the total VP fluorescence was measured by adding 100 μL acetonitrile into each dialysis device to entirely destabilise the nanoparticles. VP release percentage was determined by the following equation:

$$\text{VP release}\% = V_T/V \times 100\%$$

Where V_T is fluorescence intensity at each time point and V is fluorescence intensity after the nanoparticles were destabilised by acetonitrile.

In pH stability studies, 200 μL nanoparticle samples were incubated with MES buffer with pH at 7.5 (control), 6.0 and 5.0, respectively. Subsequently, these samples were transferred into dialysis devices, which were then kept in 50 mL centrifuge tubes containing 10 mL corresponding MES buffer, followed by the same dialysis procedure and fluorescence measurement described above.

2.2.4. Cellular uptake

Human normal colon cell line CCD841 CoN (6.92×10^5 mL^{-1}) and human colon cancer cell line HCT116 (5.86×10^5 mL^{-1}) were attached to glass-bottom petri dishes and incubated at 37 ℃ in a humidified 5%

CO_2 atmosphere with corresponding cell media comprising EMEM mixed with 10% FBS for 4 days and McCoy's 5 A mixed with 10% FBS and 1% antibiotic-antimycotic for 2 days, respectively. CCD841 CoN cells need longer culture period because the proliferation of CCD841 is much slower than HCT116 [23,24]. After removing the culture medium, the cells were incubated with nanoparticle suspension in Opti-MEM for 0.5 h, 1 h, 2 h, and 3 h. The cells were then washed with DPBS (1×, pH 7.4) three times to remove free nanoparticles. For imaging the cellular uptake of nanoparticles, 1 mL living cell imaging solution and NucBlue™ Live Ready Probes™ Reagent (5 μg mL^{-1}) were added into each petri dish, respectively. The cells were imaged using laser scanning confocal microscope (FV3000; Olympus, Tokyo, Japan). A violet laser at 405 nm was utilized for the excitation of VP and cell nucleus, respectively. All images were analysed using a UPLSAPO 40 × 2 air objective lens. Fluorescence emission was collected using filters with band pass of 680–710 nm for VP fluorescence and 430–470 nm for nucleus fluorescence. The cell fluorescence was measured using ImageJ software. The corrected total cell fluorescence (CTCF) was obtained using the following formula:

CTCF = Integrated Density - (Area of selected cell × Mean fluorescence of background readings)·

2.2.5. $^1O_2$ generation measurement in water solution

400 μL diluted nanoparticle suspension was mixed with 6 μL SOSG (0.5 mM) and the mixture was then added to regular 48-well plates in triplicate (3 different wells per group). These plates were exposed to X-ray radiation at different dose (2, 4 and 6 Gy), separately, via a 320 kV cabinet X-Ray Irradiator (X-RAD 320, Precision X-Ray, Inc., Madison, USA). The SOSG fluorescence intensity was recorded by using a plate reader (SpectraMax i3x Multi-Mode Microplate Reader, Molecular Devices, California, USA) before and after X-ray irradiation. The percentage of SOSG fluorescence intensity enhancement was calculated by the following Equation:

$$\text{Percentage enhancement } (\%) = (V_2\text{-}V_1)/V_1 \times 100\%$$

Where V_1 and V_2 represent fluorescence intensity of SOSG before and after X-ray irradiation.

2.2.6. Intracellular ROS detection

HCT116 cells (6.39 $\times 10^5$ cells/mL) were attached to glass-bottom petri dishes and incubated at 37 ℃ for 48 h. The cells were then treated with 1 mL nanoparticle suspensions (200 μL nanoparticles mixed with 800 μL Opti-MEM) for 2 h at 37 ℃, followed by cell wash with 1 mL 1 × HBSS five times. Subsequently, 200 μL of DCF-DA fluorescent probe solution (25 μM DCF-DA in 1 × HBSS) was added and incubated with cell for another 1 h at 37 ℃ in darkness. After the cells washing with fresh medium for three times, they were irradiated with 4 Gy X-ray, and then imaged under FV3000 confocal laser scanning microscope. A laser at 488 nm was used for DCF-DA excitation and the detection wavelength was 500–600 nm. Quantitative analysis of DCF-DA signal was conducted by using ImageJ software, which indicated the intracellular ROS level generated under different experimental conditions.

2.2.7. Nanoparticle toxicity assay

CCD841 CoN (5.04 × 10^5 mL^{-1}) and HCT116 cells (3.28 $\times 10^5$ cells/mL) were grown on 96-well plates in the culture medium with 10% FBS for 24 h. After removing the old media, the cells were incubated with 100 μL Opti-MEM solution containing FA-LPNPs-VP-5-FU with different concentrations for 2 h. After incubation, the old medium was removed and fresh medium was added, followed by another 24 h incubation. The nanoparticle toxicity was assessed using the MTS Cell Viability Assay Kit according to its protocol. The absorbance at the wavelength of 490 nm was measured by SpectraMax i3x Multi-Mode Microplate reader. The cell viability was calculated as a percentage of the absorbance in the treated cells compared with that of untreated cells, as follows:

$$\text{Viability } (\%) = (A_c - A_{blank})/(A_0 - A_{blank}) \times 100\%$$

where A_c is the absorbance of each group, A_0 is the absorbance of the control group, and A_{blank} is the absorbance of cell culture medium.

2.2.8. In vitro X-PDT effect on cell viability

X-PDT effect on cell viability was assessed by using MTS assay and Cell Viability Imaging kit, respectively. In brief, HCT116 cells (3 $\times 10^5$ cells/mL) were seeded into 96-well plates and incubated for 24 h. When cells reached 70% confluency, cells were treated with different nanoparticle samples for 2 h. Cells then were kept in fresh medium for X-ray radiation. At 24 h after the treatments, the cell viability was measured and calculated by using the same method as described above (Nanoparticle toxicity assay).

We also checked the cell viability by using ReadyProbes® Cell Viability Imaging Kit, Blue/Green (R37609). In this experiment, HCT116 cells (6.29 $\times 10^5$ cells/mL) were seeded to glass bottom petri dishes and incubated at 37 ℃ for 48 h. When the cells grew to 70% confluency, they were divided into groups for different treatments, cells alone, cells treated with X-ray alone, cells treated with LPNPs, LPNPs-VP, LPNPs-VP-5-FU or FA-LPNPs-VP-5-FU alone, and cells treated with LPNPs, LPNPs-VP, LPNPs-VP-5-FU or FA-LPNPs-VP-5-FU combined with X-ray. At 24 h after all treatments, the ReadyProbes® Cell Viability Imaging Kit (Blue/Green) was applied to all groups as per its manufacturer's instructions. Blue fluorescence signal (Ex/Em 360/460 nm) from the nuclei of all cells and the green fluorescence signal (Ex/Em 504/523 nm) from the nuclei of dead cells were imaged under FV3000 confocal laser scanning microscope. The cell viability was calculated as a percentage of live cell number in the treated cells compared with untreated cells, as follows:

$$\text{Viability } (\%) = (N_{\text{total}} - N_{\text{death}})/N_{\text{total}} \times 100\%$$

where N_{death} is the dead cell number, and N_{total} is the total cell number.

2.2.9. Apoptosis/necrosis assay

To discriminate among apoptotic, necrotic and live cells after X-PDT on HCT116 cells, apoptosis/necrosis assay was carried out by using an Apoptosis/Necrosis Assay Kit (ab176750). HCT116 cells (6 $\times 10^5$ cells/mL) were seeded to glass bottom petri dishes. When the cells grew to 60–70% confluency, the petri dishes were divided into groups for different treatments: cells alone; cells treated with 4 Gy X-ray alone, cells treated with LPNPs alone, LPNPs-5-FU alone, LPNPs-VP alone and FA-LPNPs-VP-5-FU alone and cells treated with LPNPs & 4 Gy, LPNPs-5-FU & 4 Gy, LPNPs-VP & 4 Gy and FA-LPNPs-VP-5-FU & 4 Gy. At 24 h after the treatments, the Apoptosis/Necrosis Assay kit was applied to the cells according to its instruction, followed by imaging the cells under Olympus FV3000 confocal laser scanning microscope. Blue fluorescence signal (Ex/Em = 405/450 nm) indicated healthy cells; green fluorescence signal (Ex/Em = 490/525 nm) implied late apoptosis and necrosis pathway of damaged cells; red fluorescence signal (Ex/Em = 630/660 nm) represented apoptosis pathway of cell death. The data was analysed by counting the number of healthy/apoptotic/necrotic cells and comparing with total cells, as follows:

$$\text{Healthy/apoptotic/necrotic cells } (\%) = N_{\text{healthy/apoptotic/necrotic cells}}/N_{\text{total}} \times 100\%$$

where $N_{\text{healthy/apoptotic/necrotic cells}}$ is the number of healthy/apoptotic/necrotic cells of each group, and N_{total} is the total cell number of this group.

2.2.10. Cell cycle assay

To confirm whether X-PDT and other treatment conditions induce

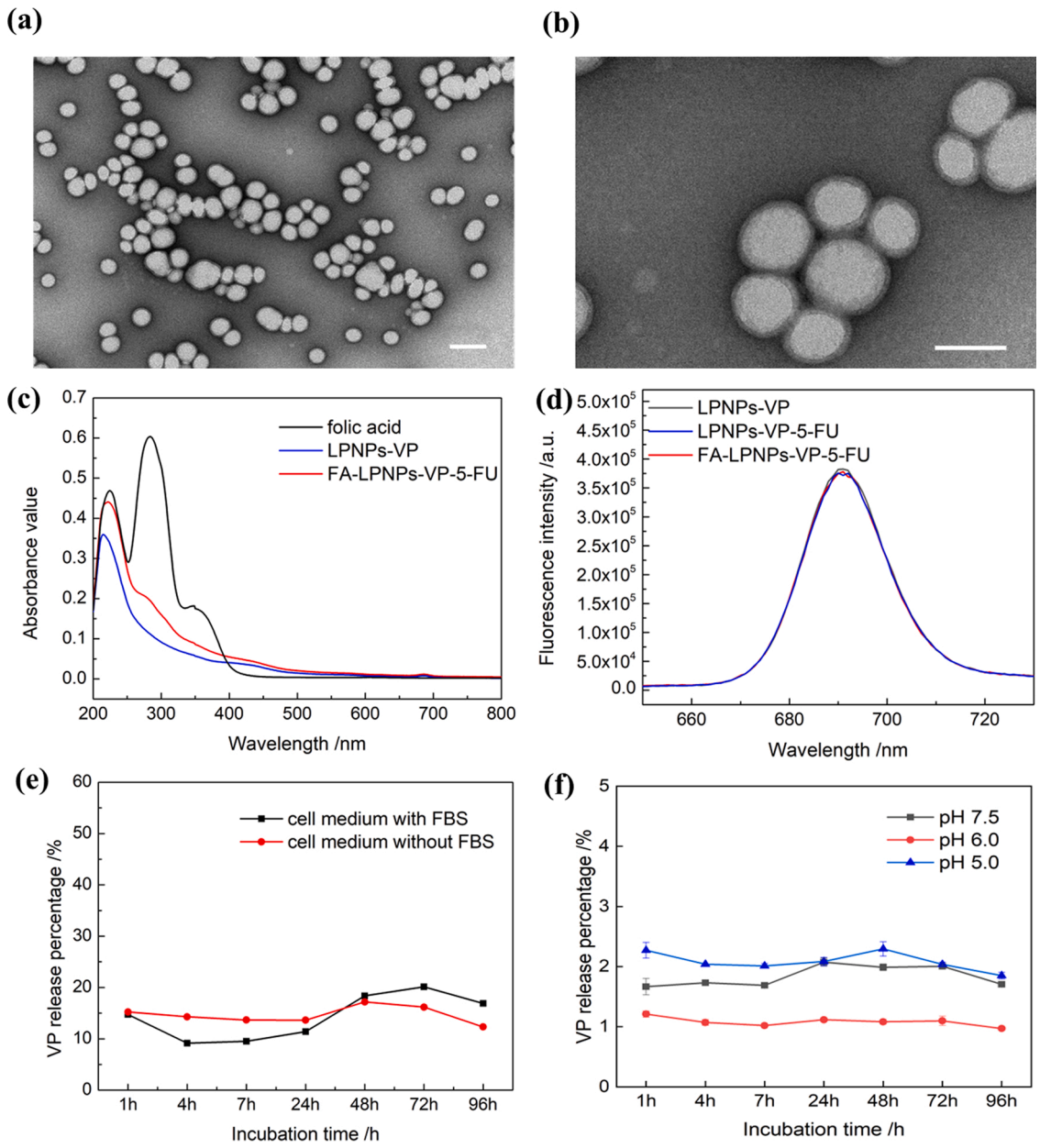

Fig. 1. Nanoparticles characterization (a) and (b) The TEM images of FA-LPNPs-VP-5-FU, 200 nm and 100 nm; (c) UV-Vis absorbance spectra of folic acid, LPNPs-VP and FA-LPNPs-VP-5-FU; (d) The fluorescence spectra (fluorescence intensity) of LPNPs-VP, LPNPs-VP-5-FU and FA-LPNPs-VP-5-FU; (e and f): VP release profile from FA-LPNPs-VP-5-FU in FBS and different pH buffers.

cell cycle arrest in HCT116 cells, Luminex Muse Cell Cycle Kit was applied according to its manufacturer instruction. Briefly, HCT116 cells were seeded in 6-well plates (5×10^5 cells/mL) and cultured for 3 days. Afterwards, cells were divided into different groups for the following treatments: cells only, cells treated with 4 Gy X-ray only, LPNPs-5-FU only, FA-LPNPs-VP-5-FU only and cells treated with FA-LPNPs-VP-5-FU combined with 4 Gy X-ray. At 24 h after treatment, cells were harvested by trypsinization, washed once with cold DPBS, and fixed with ice-cold 70% ethanol at − 20 ℃ for at least 3 h. After fixation, the cells were washed once with DPBS and suspended in 200 μL Muse® Cell Cycle reagent for 30 min at room temperature in darkness. Cell cycle phase distribution was measured by Muse® Cell Analyzer (Luminex Corporation, Texas, USA).

2.2.11. Statistical analysis

All quantitative data are shown as mean ± SD, n ≥ 3. Statistical analysis was conducted by using Origin 8.5 software. *p < 0.05; * *p < 0.01; * **p < 0.005.

3. Results and discussion

3.1. Characterisation of prepared lipid-polymer hybrid nanoparticles

In this study, the lipid-polymer hybrid nanoparticles were prepared with a hydrophobic PLGA core for the encapsulating VP and 5-FU, a hydrophilic DSPE-PEG stealth shell, and a lipid monolayer (lecithin) between the PLGA core and DSPE-PEG shell through a single-step nanoprecipitation method. The particle size was firstly investigated using TEM. As shown in Fig. 1(a), the average size of FA-LPNPs-VP-5-FU was about 100 nm, and the core/shell structure was clearly observed under high magnification (Fig. 1(b)).

Furthermore, we investigated the particle size and zeta potential

Table 2
The average size, zeta potential, polydispersity and EE% of VP and 5-FU for as-prepared nanoparticles in deionized water.

Samples	Zeta (mV)	Size (d. nm)	Polydispersity	EE% of VP	EE% of 5-FU
LPNPs	-48.6 ± 3.1	98.5 ± 2.1	0.11 ± 0.03	–	–
LPNPs-VP	-46.3 ± 5.0	101.0 ± 2.6	0.17 ± 0.01	92.49 ± 0.18	–
LPNPs-5-FU	-35.5 ± 0.4	98.0 ± 1.3	0.14 ± 0.02	–	7.30 ± 0.35
LPNPs-VP-5-FU	-38.2 ± 0.5	100.5 ± 1.7	0.14 ± 0.02	94.14 ± 1.22	4.73 ± 0.89
FA-LPNPs-VP-5-FU	-32.5 ± 2.2	101.7 ± 2.1	0.16 ± 0.02	93.07 ± 0.56	4.52 ± 1.06

using dynamic light scattering system (Table 2). The average particle size of these samples was about 100 ± 3 nm which is compatible with the size from TEM images. The zeta potential (ζ) of all these samples was negatively charged and it slightly increased after 5-FU loading or folic acid modification. The low polydispersity index indicates that all samples are monodisperse. In addition, the encapsulation efficiency (EE%) of drugs from each nanoparticle sample was investigated (Table 2), and superior encapsulation efficiency of VP (over 90%) in LPNPs-VP, LPNPs-VP-5-FU and FA-LPNPs-VP-5-FU were observed. Moreover, the encapsulation efficiency of 5-FU in LPNPs-5-FU, LPNPs-VP-5-FU and FA-LPNPs-VP-5-FU were investigated, and compatible results with previous studies was observed [25,26]. The relatively low loading capacity of 5-FU (5–8%) is tentatively attributed to hydrophilicity of 5-FU which may lead to immediate diffusion of 5-FU to the aqueous phase during the preparation process.

In order to confirm the existence of folic acid in nanoparticles, we measured and analysed the absorbance spectra of folic acid, LPNPs and FA-LPNPs-VP-5-FU, as shown in Fig. 1(c). The characteristic absorption peak of folic acid is around the wavelength of 282 nm, which is observed in FA-LPNPs-VP-5-FU, but this peak was not present in the absorption spectra of LPNPs, confirming incorporation of folic acid in lipid-polymer hybrid nanoparticles, and it is consistent with the peak location in published work [27]. In addition, we measured the fluorescence emission intensity from VP of LPNPs-VP, LPNPs-VP-5-FU and FA-LPNPs-VP-5-FU at the excitation wavelength of 425 nm (Fig. 1(d)). The fluorescence values of VP at the emission wavelength of 690 nm of LPNPs-VP, LPNPs-VP-5-FU and FA-LPNPs-VP-5-FU are all similar, which also indicates a similar concentration of VP encapsulated in these nanoparticle samples.

Furthermore, the stability of FA-LPNPs-VP-5-FU to FBS and different pH buffers were investigated by assessing VP release from these samples via dialysis technique. Fig. 1(e) confirmed that FA-LPNPs-VP-5-FU exhibited the similar VP release profile with and without the present of FBS in the cell medium. Fig. 1(f) demonstrated that stability of nanoparticles was not affected by pH value ranging from 5.0 to 7.5, with less than 3% of VP being released at 96 h. All these findings indicated that our nanoparticles were sufficiently stable under the current experiment conditions, without major drug leaking out of its carriers.

3.2. Cellular uptake of targeted nanoparticles

In order to realize exceptional targeting effect of our nanoparticles on CRC, a folic acid modification approach was introduced to immobilize folic acid molecules on the surface of nanoparticles, since folate receptor is known to be overexpressed approximately 38% of CRC cells (such as HCT116 cells), comparing to normal human colon cells [28]. This approach is an effective strategy for active targeting of CRC in drug delivery systems, achieving increased cellular accumulation of drugs and enhanced treatment efficacy [29,30]. By taking advantage of this targeting strategy, we modified nanoparticles by using the DSPE-PEG-FA to partly replace DSPE-PEG in the formulation. The targeting capability of FA-LPNPs-VP-5-FU was investigated by assessing and comparing their cellular uptake activities in human colon cancer cell line HCT116 cells and human normal colon cell line CCD841 CoN (controls). Further we also evaluated the targeted (FA-LPNPs-VP-5-FU) and non-targeted

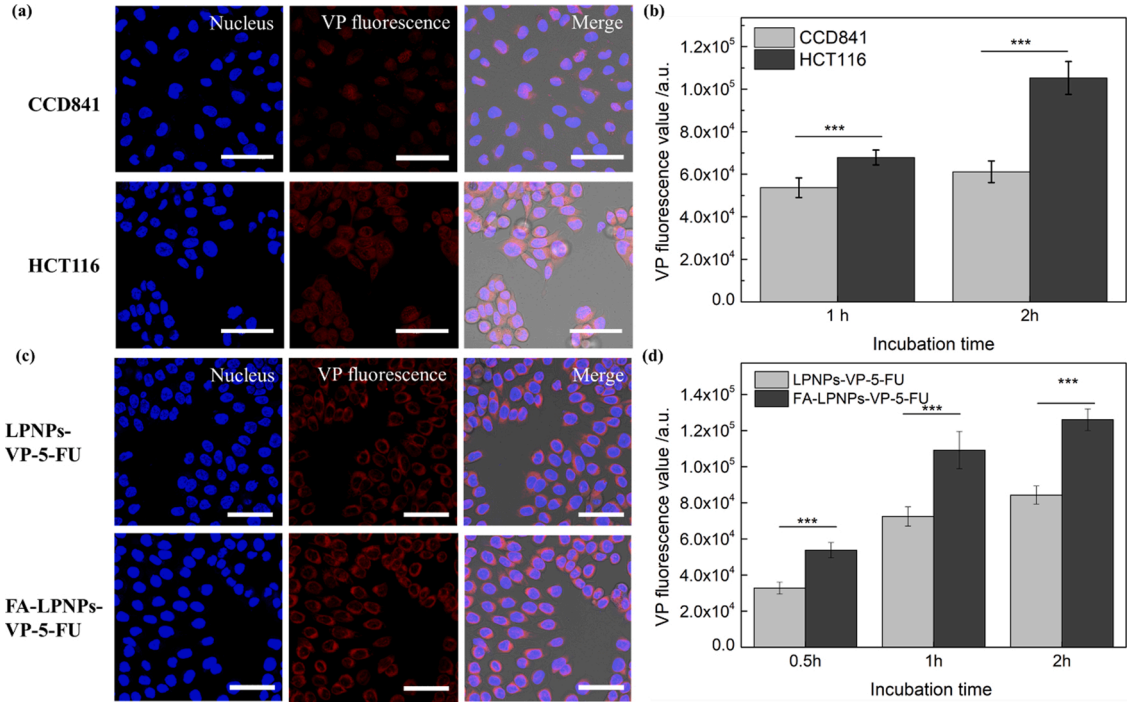

Fig. 2. (a) Confocal microscope images of HCT116 cells and CCD841 CoN cells after incubation with FA-LPNPs-VP-5-FU; (b) VP fluorescence intensity from FA-LPNPs-VP-5-FU in HCT116 cells and CCD841 CoN cells at different incubation period; (c) Confocal microscope images of HCT116 cells after 2 h incubation with FA-LPNPs-VP-5-FU and LPNPs-VP-5-FU; (d) VP fluorescence intensity from FA-LPNPs-VP-5-FU and LPNPs-VP-5-FU in HCT116 cells at different incubation period. The scale bar is 60 μm. The calculated area of each sample contained about 60 cells. *p < 0.05; * *p < 0.01; * **p < 0.005.

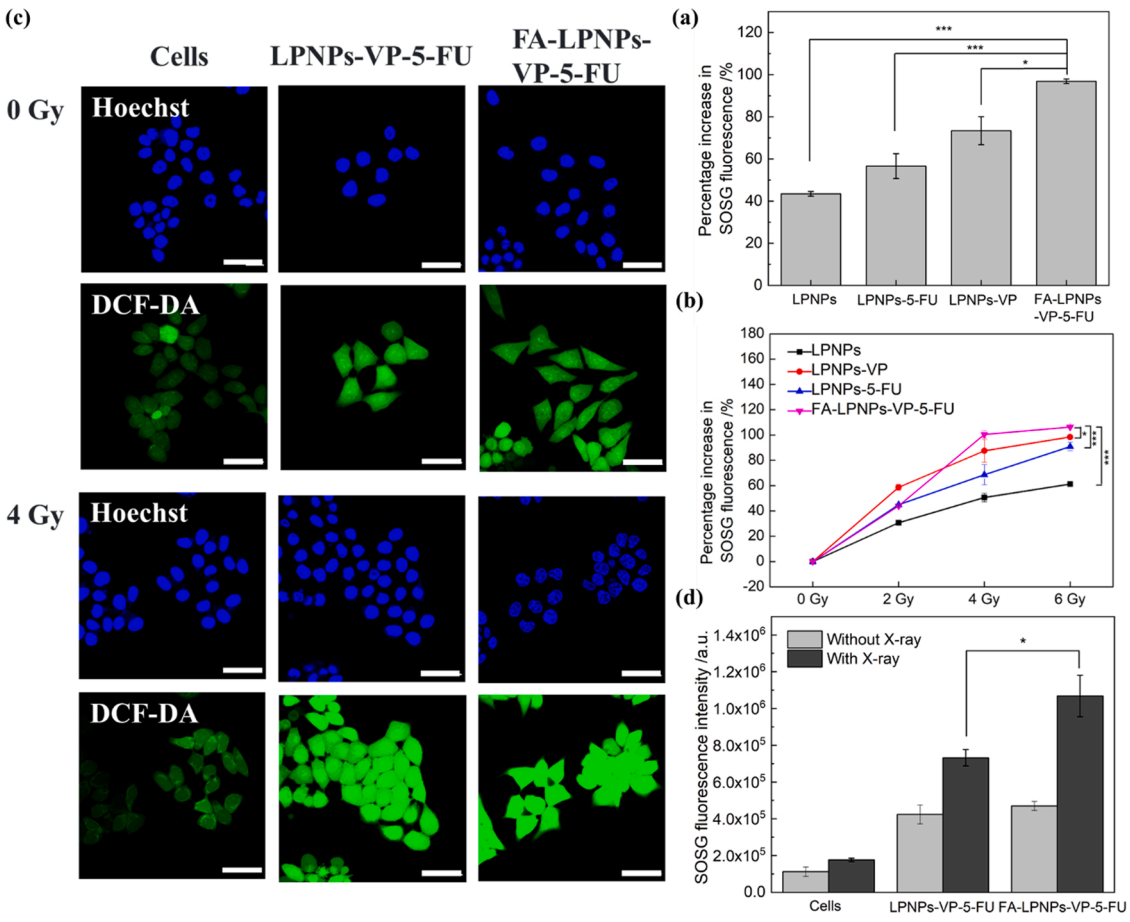

Fig. 3. (a) The increase percentage of SOSG fluorescence intensity from different nanoparticle samples under 4 Gy irradiation; (b) The increase percentage of SOSG intensity measured in different nanoparticle samples under different X-ray dose; (c) Intracellular ROS generation from nanoparticle samples with and without X-ray treatment, scar bar 200 μm; (d) Quantitative analysis of ROS production in HCT116 cells under different treatment conditions. (n = 3, Mean ± SD). *p < 0.05; * *p < 0.01; * **p < 0.005.

nanoparticles (LPNPs-VP-5-FU) in HCT116 cells.

As shown in Fig. 2(a) and Supplementary Fig. 1, VP fluorescence from FA-LPNPs-VP-5-FU was slightly higher in HCT116 than CCD841 cells after 1 h incubation, with enhancement factor of 1.26 (Fig. 2b). At 2 h incubation, HCT116 cells treated with FA-LPNPs-VP-5-FU clearly exhibited the red signal from VP (1.72 times higher signal in Fig. 2b), compared with CCD841 cells. Additionally, we also evaluated the cellular uptake of FA-LNPs-VP-5-FU and non-targeted LPNPs-VP-5-FU by HCT116 at different incubation times (Fig. 2c and d). As shown in Fig. 2(d), VP fluorescence intensity from FA-LPNPs-VP-5-FU exhibited about 1.64 times, 1.51 times and 1.49 times higher than non-targeted counterparts at 0.5 h, 1 h and 2 h incubation time, respectively. The corresponding confocal images were provided in Supplementary Fig. 2 (0.5 h and 1 h). These results are in good agreement with previous reports [12,31], indicating that folic acid may bind to the folate receptor which is highly expressed on HCT116 cell surface and resulted in a higher internalisation rate of FA-LPNPs-VP-5-FU, compared to the normal CCD841 CoN cells and non-targeted LPNPs-VP-5-FU.

3.3. $^1O_2$ and ROS generation measurement

3.3.1. $^1O_2$ generation measurement after X-ray treatment in solution

The main factor responsible for the PDT effect is the generation of cytotoxic ROS, such as $^1O_2$. In this study, the generation of $^1O_2$ was confirmed by using a $^1O_2$ indicator SOSG probe, which emits a strong green fluorescence signal at 525 nm for 488 nm excitation in the presence of $^1O_2$ [32]. Among the tested nanoparticles, FA-LPNPs-VP-5-FU produced the highest amount of $^1O_2$, with an increase of approximately 97% under X-ray irradiation at 4 Gy (Fig. 3(a)). In addition, we also investigated the impact of X-ray doses on the generation of $^1O_2$ (Fig. 3(b)). Among these nanoparticles, the SOSG intensity initially grew with increase in X-ray radiation dose from 0 to 4 Gy. The highest SOSG fluorescence intensity was observed in FA-LPNPs-VP-5-FU at 4 Gy radiation, compared with other samples, while it reached a plateau at 6 Gy. Thus, 4 Gy was the optimum value for further intracellular ROS measurement.

3.3.2. Detection of intracellular ROS generation after X-ray treatment

After confirmation of $^1O_2$ generation in solution, we further detected the intracellular ROS generation under different treatment conditions via DCF-DA assay. In principle, the DCF-DA molecules are cell penetrable and can be oxidized by ROS, leading to the generation of fluorescent DCF [33]. As shown in Fig. 3(c) and (d), the DCF-DA fluorescence intensity measured in the cells treated with 4 Gy X-ray radiation did not exhibit significant difference, compared with the control cells. This indicates that the 4 Gy dose did not trigger the sufficient ROS production in these cells. A similar amount of ROS was observed in the cell groups treated with LPNPs-VP-5-FU and FA-LPNPs-VP-5-FU alone. When combined with X-ray radiation, the cells treated with these nanoparticles exhibited a clearly higher ROS amount (6.5 folds and 9.5 folds fluorescence intensity compared with control cells, respectively). The confocal images of cell groups treated with LPNPs, LPNPs-VP and LPNPs-5-FU were also showed in Supplementary Fig. 3. Interestingly, the cell group treated with LPNPs-5-FU

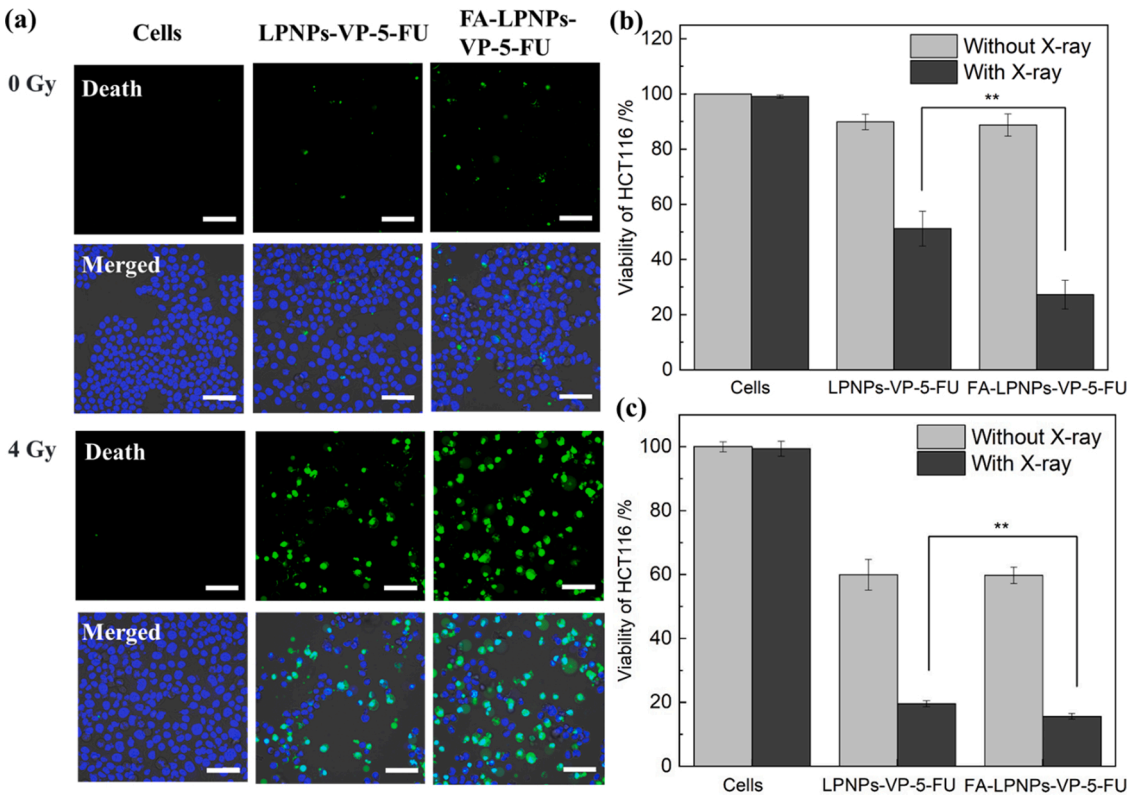

Fig. 4. HCT116 cell viability analysis under different treatment conditions. (a) and (b) The confocal microscopy images of cells exposed to different treatment conditions and quantitative analysis by ImageJ software. Scale bar, 200 μm. Green fluorescence signals represented dead cells; (c) The calculated cell viability percentage at 24 h by conducting MTS assay. (n = 3, Mean ± SD). *p < 0.05; * *p < 0.01; * **p < 0.005.

also showed the higher amount of ROS generation compared with LPNPs (Supplementary Fig. 3). This could be attributed to the mitochondrial ROS generation by 5-FU [34–36]. Collectively taken, FA-LPNPs-VP-5-FU combined with 4 Gy radiation produced the highest intracellular ROS amount among these samples.

3.4. Evaluation of in vitro X-PDT effect on cell viability

Before assessing the in vitro X-PDT effect, we investigated the dark toxicity of FA-LPNPs-VP-5-FU in HCT116 and CCD841 CoN cells by the MTS assay. HCT116 cells remains over 70% survival at 24 h after incubation with 186.8 μg/mL of FA-LPNPs-VP-5-FU (Supplementary Fig. 4). Also, as shown in Supplementary Fig. 5, FA-LPNPs-VP-5-FU nanoparticles exhibited lower cell toxicity towards CCD841 CoN cells than HCT116 cells (cell viability, 83.85% v.s 70.94%) at this concentration. This could be attributed to higher internalisation of FA-LPNPs-VP-5-FU in HCT116 than in CCD841 CoN cells, as we demonstrated in Fig. 2. Based on these findings, we chose this concentration for further X-PDT effect evaluation.

We first conducted the cell viability by imaging and counting live vs.

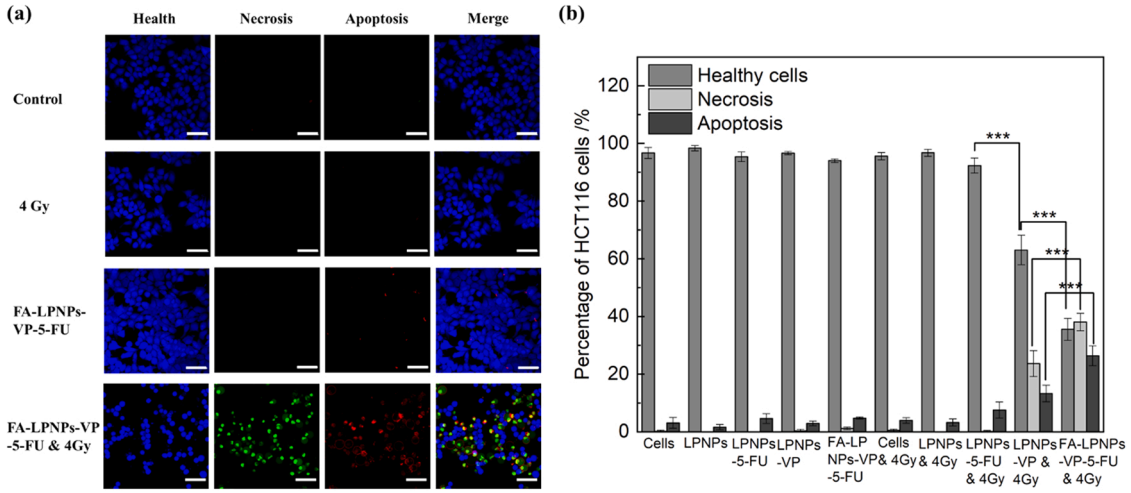

Fig. 5. Apoptosis/necrosis assays conducted in HCT116 cells at 24 h after various treatments. (a) Representative confocal microscopy images of cells. Blue (CytoCalcein Violet 450), healthy cells; green (DNA Nuclear Green DCS1Dye), necrotic cells and red (Apopxin Deep Red Indicator), apoptotic cells. Scar bar, 200 μm; (b) The cell percentage changes in levels of apoptosis/necrosis (n = 3, Mean ± SD). *p < 0.05; * *p < 0.01; * **p < 0.005.

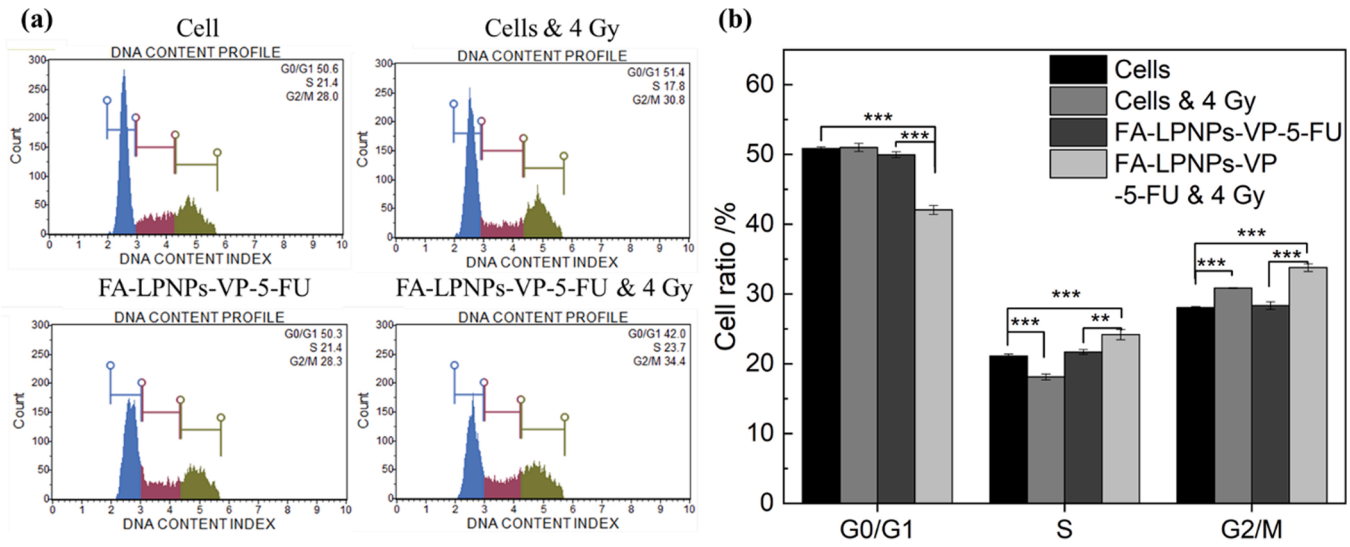

Fig. 6. (a) HCT116 cell cycle distribution at 24 h after various treatment conditions; (b) The percentage of HCT116 cells at G0/G1, S and G2/M phases after 24 h. (n = 3, Mean ± SD). *p < 0.05; * *p < 0.01; * **p < 0.005.

dead cells. From the confocal images of cells and data analysis (Fig. 4(a), (b) and Supplementary Fig. 6), 4 Gy radiation alone and nanoparticles alone did not produce the major cytotoxicity in HCT116 cells, compared with control group. However, significant decrease in cell viability was observed when treated with 4 Gy X-ray radiation combined with LPNPs-VP-5-FU and FA-LPNPs-VP-5-FU, being 51 ± 6% and 27 ± 5% of cells alive, respectively. These findings implied that 5-FU loaded in these nanocarriers could enhance X-ray radiation [17–19], generating more ROS and subsequently higher cytotoxicity effect (Fig. 4(b)). The MTS assay also shows a similar trend under the same treatment conditions, with only 20 ± 1% and 16 ± 1% of cells alive after the combined treatments, respectively (Fig. 4(c)). These results were consistent with our previous data regarding cellular uptake and intracellular ROS generation, verifying that the enhanced cytotoxicity effect is a result of folate-induced targeting uptake and a combined effect of efficient ROS production under X-ray radiation and chemo-drugs. In comparison with previous reports [12,37], the X-PDT effect (about 84% cytotoxicity) in our study was higher than FA-PLGA-VP which contains VP (67% cytotoxicity) and $^{DA}NP_{VP\&DOX}$ which coloaded with VP and doxorubicin (63% cytotoxicity). The possible reason could be attributed to smaller nanoparticle size and higher encapsulation efficiency of VP in our study, compared with FA-PLGA-VP (about 250 nm and 65% EE% of VP) and $^{DA}NP_{VP\&DOX}$ (about 120 nm and 51% EE% of VP).

3.5. Apoptosis/necrosis assays

The HCT116 cell death pathway after the treatment conditions was further investigated by Apoptosis/Necrosis assays. As displayed in Fig. 5, compared with the control group (cells alone), the cells treated with X-ray irradiation alone, LPNPs, LPNPs-5-FU, LPNPs-VP and FA-LPNPs-VP-5-FU without X-ray radiation exhibited similar low-level apoptosis and necrosis. This indicated that 4 Gy X-ray irradiation, pure nanocarriers, LPNPs-5-FU and LPNPs-VP and FA-LPNPs-VP-5-FU alone at current concentration showed negligible cytotoxicity to cells and the limited antitumour effect. However, the maximum percentage of apoptosis and necrosis was observed in the cell group treated with FA-LPNPs-VP-5-FU & 4 Gy, being 26 ± 3% and 38 ± 3%, respectively. Correspondingly, the percentage of healthy cells in this group reduced to about 36 ± 3%, compared to cell control group (accounting for 97 ± 2%). The representative confocal images of apoptotic and necrotic cells after treatments with LPNPs, LPNPs-5-FU and LPNPs-VP were showed in Supplementary Fig. 7. Taken together, these findings indicate that X-PDT effect triggered the cancer cell death via apoptosis and necrosis pathway. These results are consistent with our findings on intracellular ROS generated with FA-LPNPs-VP-5-FU & 4 Gy (Fig. 3 and Supplementary Fig. 3) and previously published studies where ROS induced apoptosis and necrosis to inhibit cancer cells proliferation with X-PDT treatment [11,37,38].

3.6. Cell cycle assays

Cell cycle dysfunction is closely related to cancer development, and any interference in cell cycle progression will potentially cause apoptotic cell death [39,40]. To analysis whether X-PDT-induced growth inhibition and apoptosis of HCT116 cells was mediated through cell cycle arrest, we further examined the effects of our treatment on cell cycle distribution. Fig. 6 and Supplementary Fig. 8 displayed the cell cycle distribution of control group (cells only), cells treated with 4 Gy X-ray, LPNPs-5-FU alone, FA-LPNPs-VP-5-FU alone and combined condition of FA-LPNPs-VP-5-FU & 4 Gy X-ray. Fig. 6 showed that combined treatment (FA-LPNPs-VP-5-FU & 4 Gy X-ray) on HCT116 cells led to a higher population in S-phase and G2/M phase, whereas the proportion of cells at G0/G1 phase decreased significantly compared with untreated cells or cells treated FA-LPNPs-VP-5-FU alone. Interestingly, the cell groups treated with X-ray only showed a decreased percentage of cell in S-phase, but slight increase in G2/M phase, compared with control cells. This indicates that DNA damage repair following irradiation happened, resulting in G2/M phase arrest, which is an indicator of cellular radiosensitivity [41,42]. Overall, the results suggest that X-PDT effectively inhibits HCT116 cell proliferation via G2/M and S phase arrest, which leads to cellular apoptosis.

4. Conclusion

In summary, we have developed a folic acid modified lipid-polymer hybrid nanoparticle delivery system which combines X-PDT and chemo-drug to treat CRC cells. The nanoparticles were formulated by co-loading VP and 5-FU in the same platform and modified with folic acid (FA-LPNPs-VP-5-FU). FA-LPNPs-VP-5-FU exhibited in vitro CRC targeting capacity and produced sufficient ROS under 4 Gy X-ray irradiation. Cellular assessment demonstrated that FA-LPNPs-VP-5-FU in combination with 4 Gy radiation effectively inhibited HCT116 cells growth, led cell death through apoptosis and necrosis pathway and interfered cell division at G2/M and S phase. Collectively, these results indicated this nanoparticle delivery system may provide the feasibility of new treatment for CRC with the combined chemo-drugs and low dose X-ray

radiation.

CRediT authorship contribution statement

Rui Sang: Conceptualization, Data curation, Methodology, Formal analysis, Investigation, Writing – original draft, Writing – review & editing, Funding acquisition. **Fei Deng:** Formal analysis, Writing – review & editing. **Alexander Engel:** Writing – review & editing. **Ewa Goldys:** Conceptualization, Project administration, Resources, Funding acquisition, Supervision, Writing – review & editing. **Wei Deng:** Conceptualization, Methodology, Project administration, Resources, Funding acquisition, Supervision, Writing – review & editing.

Data Availability

Data will be made available on request.

Acknowledgments and funding

We acknowledge Electron Microscope Init at Mark Wainwright Analytical Centre in UNSW for helping us with the TEM images. This work was financially supported by the funding (GNT1181889) from the Australian National Health and Medical Research Council, fellowship award (2019/CDF1013) from Cancer Institute NSW, Australia, the Australian Research Council Centre of Excellence for Nanoscale Biophotonics (CE140100003), UNSW SHARP funding, PhD Research Scholar Award from Sydney Vital Translational Cancer Research, and Translational Cancer Research Network PhD Scholarship Top-up award.

Conflict of interest statement

The authors report no conflicts of interest in this work. Wei Deng and Ewa Goldys are co-directors, and they hold shares in companies Radiodynamic Therapeutics Pty Ltd and Theragenos Pty Ltd developing a similar type of drug delivery vehicles.

Appendix A. Supporting information

Supplementary data associated with this article can be found in the online version at doi:10.1016/j.biopha.2022.113837.

References

[1] H. Sung, J. Ferlay, R.L. Siegel, M. Laversanne, I. Soerjomataram, A. Jemal, F. Bray, Global Cancer Statistics 2020: GLOBOCAN Estimates of Incidence and Mortality Worldwide for 36 Cancers in 185 Countries, CA: Cancer J, Clin 71 (3) (2021) 209–249, https://doi.org/10.3322/caac.21660.

[2] K.D. Miller, L. Nogueira, A.B. Mariotto, J.H. Rowland, K.R. Yabroff, C.M. Alfano, A. Jemal, J.L. Kramer, R.L. Siegel, Cancer treatment and survivorship statistics, 2019, CA: Cancer J, Clin 69 (5) (2019) 363–385, https://doi.org/10.3322/caac.21565.

[3] R. Sang, B. Stratton, A. Engel, W. Deng, Liposome technologies towards colorectal cancer therapeutics, Acta Biomater. 127 (2021) 24–40, https://doi.org/10.1016/j.actbio.2021.03.055.

[4] M.D. Hellinger, C.A. Santiago, Reoperation for recurrent colorectal cancer, Clin. Colon Rectal Surg. 19 (4) (2006) 228–236, https://doi.org/10.1055/s-2006-956445.

[5] A. Riaz, R. Awais, R. Salem, Side effects of yttrium-90 radioembolization, Front. Oncol. 4 (2014) 198, https://doi.org/10.3389/fonc.2014.00198.

[6] L. Chintala, S. Vaka, J. Baranda, S.K. Williamson, Capecitabine versus 5-fluorouracil in colorectal cancer: where are we now? Oncol. Rev. 5 (2) (2011) 129–140, https://doi.org/10.1007/s12156-011-0074-3.

[7] M. Lan, S. Zhao, W. Liu, C.S. Lee, W. Zhang, P. Wang, Photosensitizers for photodynamic therapy, Adv. Healthc. Mater. 8 (13) (2019), e1900132, https://doi.org/10.1002/adhm.201900132.

[8] M.Q. Mesquita, C.J. Dias, S. Gamelas, M. Fardilha, M. Neves, M.A.F. Faustino, An insight on the role of photosensitizer nanocarriers for Photodynamic Therapy, . Acad. Bras. Cienc. 90 (1 Suppl 2) (2018) 1101–1130, https://doi.org/10.1590/0001-3765201720170800.

[9] J. Chen, T. Fan, Z. Xie, Q. Zeng, P. Xue, T. Zheng, Y. Chen, X. Luo, H. Zhang, Advances in nanomaterials for photodynamic therapy applications: Status and challenges, Biomaterials 237 (2020), 119827, https://doi.org/10.1016/j.biomaterials.2020.119827.

[10] X.D. Ren, X.Y. Hao, H.C. Li, M.R. Ke, B.Y. Zheng, J.D. Huang, Progress in the development of nanosensitizers for X-ray-induced photodynamic therapy, Drug Discov. Today 23 (10) (2018) 1791–1800, https://doi.org/10.1016/j.drudis.2018.05.029.

[11] W. Deng, K.J. McKelvey, A. Guller, A. Fayzullin, J.M. Campbell, S. Clement, A. Habibalahi, Z. Wargocka, L. Liang, C. Shen, V.M. Howell, A.F. Engel, E. M. Goldys, Application of mitochondrially targeted nanoconstructs to neoadjuvant X-ray-induced photodynamic therapy for rectal cancer, ACS Cent. Sci. 6 (5) (2020) 715–726, https://doi.org/10.1021/acscentsci.9b01121.

[12] S. Clement, W. Chen, W. Deng, E.M. Goldys, X-ray radiation-induced and targeted photodynamic therapy with folic acid-conjugated biodegradable nanoconstructs, Int. J. Nanomed. 13 (2018) 3553–3570, https://doi.org/10.2147/IJN.S164967.

[13] S. Clement, A.G. Anwer, L. Pires, J. Campbell, B.C. Wilson, E.M. Goldys, Radiodynamic therapy using TAT peptide-targeted verteporfin-encapsulated PLGA nanoparticles, Int. J. Mol. Sci. 22 (12) (2021) 6425, https://doi.org/10.3390/ijms22126425.

[14] K. Brodowska, A. Al-Moujahed, A. Marmalidou, M.M. Zu Horste, J. Cichy, J. W. Miller, E. Gragoudas, D.G. Vavvas, The clinically used photosensitizer Verteporfin (VP) inhibits YAP-TEAD and human retinoblastoma cell growth in vitro without light activation, Exp. Eye Res. 124 (2014) 67–73, https://doi.org/10.1016/j.exer.2014.04.011.

[15] W. Sun, L. Luo, Y. Feng, Y. Cai, Y. Zhuang, R.J. Xie, X. Chen, H. Chen, Aggregation-induced emission gold clustoluminogens for enhanced low-dose X-ray-induced photodynamic therapy, Angew. Chem. Int. Ed. Engl. 59 (25) (2020) 9914–9921, https://doi.org/10.1002/ange.201908712.

[16] S. Afzal, S. Jensen, B. Vainer, U. Vogel, J. Matsen, J. Sørensen, P. Andersen, H. Poulsen, MTHFR polymorphisms and 5-FU-based adjuvant chemotherapy in colorectal cancer, Ann. Oncol. 20 (10) (2009) 1660–1666, https://doi.org/10.1093/annonc/mdp046.

[17] E. Ojima, Y. Inoue, H. Watanabe, J. Hiro, Y. Toiyama, C. Miki, M. Kusunoki, The optimal schedule for 5-fluorouracil radiosensitization in colon cancer cell lines, Oncol. Rep. 16 (5) (2006) 1085–1091, https://doi.org/10.3892/or.16.5.1085.

[18] G. Valdes, K.S. Iwamoto, Re-evaluation of cellular radiosensitization by 5-fluorouracil: High-dose, pulsed administration is effective and preferable to conventional low-dose, chronic administration, Int. J. Radiat. Biol. 89 (10) (2013) 851–862, https://doi.org/10.3109/09553002.2013.797620.

[19] M.E. Urick, E.J. Chung, W.P. Shield, N. Gerber, A. White, A. Sowers, A. Thetford, K. Camphausen, J. Mitchell, D.E. Citrin, Enhancement of 5-fluorouracil-induced in vitro and in vivo radiosensitization with MEK inhibition5-fluorouracil radiosensitization augmented by selumetinib, Clin. Cancer Res 17 (15) (2011) 5038–5047, https://doi.org/10.1158/1078-0432.CCR-11-0358.

[20] N. Patel, L. Ghali, I. Roitt, L.P. Munoz, R. Bayford, Exploiting the efficacy of Tyro3 and folate receptors to enhance the delivery of gold nanoparticles into colorectal cancer cells in vitro, Nanosc. Adv. 3 (18) (2021) 5373–5386, https://doi.org/10.1039/D1NA00318F.

[21] L. Zhang, J.M. Chan, F.X. Gu, J.W. Rhee, A.Z. Wang, A.F. Radovic-Moreno, F. Alexis, R. Langer, O.C. Farokhzad, Self-assembled lipid–polymer hybrid nanoparticles: a robust drug delivery platform, ACS Nano 2 (8) (2008) 1696–1702, https://doi.org/10.1021/nn800275r.

[22] M.B. Zheng, P. Gong, D.X. Jia, C.F. Zheng, Y.F. Ma, L.T. Cai, Plga-lecithin-peg core-shell nanoparticles for cancer targeted therapy, Nano. Life 2 (1) (2012), 1250002, https://doi.org/10.1142/S1793984411000359.

[23] A. De Giani, F. Bovio, M. Forcella, P. Fusi, G. Sello, P. Di Gennaro, Identification of a bacteriocin-like compound from Lactobacillus plantarum with antimicrobial activity and effects on normal and cancerogenic human intestinal cells, AMB Express 9 (1) (2019) 1–11, https://doi.org/10.1186/s13568-019-0813-6.

[24] G. Li, C. Nelsen, E.A. Hendrickson, Ku86 is essential in human somatic cells, Proc. Natl. Acad. Sci. 99 (2) (2002) 832–837, https://doi.org/10.1073/pnas.022649699.

[25] M.M. El-Hammadi, A.V. Delgado, C. Melguizo, J.C. Prados, J.L. Arias, Folic acid-decorated and PEGylated PLGA nanoparticles for improving the antitumour activity of 5-fluorouracil, Int. J. Pharm. 516 (1–2) (2017) 61–70, https://doi.org/10.1016/j.ijpharm.2016.11.012.

[26] A. Russo, S. Maiolino, V. Pagliara, F. Ungaro, F. Tatangelo, A. Leone, G. Scalia, A. Budillon, F. Quaglia, G. Russo, Enhancement of 5-FU sensitivity by the proapoptotic rpL3 gene in p53 null colon cancer cells through combined polymer nanoparticles, Oncotarget 7 (48) (2016) 79656–79673, https://doi.org/10.18632/oncotarget.13216.

[27] P. Rathinaraj, K. Lee, S.Y. Park, I.K. Kang, Targeted images of KB cells using folate-conjugated gold nanoparticles, Nanoscale Res. Lett. 10 (1) (2015) 1–10, https://doi.org/10.1186/s11671-014-0725-y.

[28] J.P. Tiernan, S.L. Perry, E.T. Verghese, N.P. West, S. Yeluri, D.G. Jayne, T. A. Hughes, Carcinoembryonic antigen is the preferred biomarker for in vivo colorectal cancer targeting, Br. J. Cancer 108 (3) (2013) 662–667, https://doi.org/10.1038/bjc.2012.605.

[29] A. Grigoletto, G. Martinez, D. Gabbia, T. Tedeschini, M. Scaffidi, S. Martin, G. Pasut, Folic acid-targeted paclitaxel-polymer conjugates exert selective cytotoxicity and modulate invasiveness of colon cancer cells, Pharmaceutics 13 (7) (2021) 929, https://doi.org/10.3390/pharmaceutics13070929.

[30] S. Sarwar, M. Abdul Qadir, R.D. Alharthy, M. Ahmed, S. Ahmad, M. Vanmeert, M. U. Mirza, A. Hameed, Folate conjugated polyethylene glycol probe for tumor-targeted drug delivery of 5-fluorouracil, Molecules 27 (6) (2022) 1780, https://doi.org/10.3390/molecules27061780.

[31] P.S. Mirzaghavami, S. Khoei, S. Khoee, S. Shirvalilou, Folic acid-conjugated magnetic triblock copolymer nanoparticles for dual targeted delivery of 5-fluorouracil to colon cancer cells, Cancer Nanotechnol. 13 (1) (2022) 1–18, https://doi.org/10.1186/s12645-022-00120-3.

[32] S. Kim, M. Fujitsuka, T. Majima, Photochemistry of singlet oxygen sensor green, J. Phys. Chem. B 117 (45) (2013) 13985–13992, https://doi.org/10.1021/jp406638g.
[33] X.P. Chen, Z.F. Zhong, Z.T. Xu, L.D. Chen, Y.T. Wang, 2 ',7 '-Dichlorodihydrofluorescein as a fluorescent probe for reactive oxygen species measurement: Forty years of application and controversy, Free Radic. Res. 44 (6) (2010) 587–604, https://doi.org/10.3109/10715761003709802.
[34] P.M. Hwang, F. Bunz, J. Yu, C. Rago, T.A. Chan, M.P. Murphy, G.F. Kelso, R. A. Smith, K.W. Kinzler, B. Vogelstein, Ferredoxin reductase affects p53-dependent, 5-fluorouracil–induced apoptosis in colorectal cancer cells, Nat. Med. 7 (10) (2001) 1111–1117, https://doi.org/10.1038/nm1001-1111.
[35] J. Guo, Z. Yu, D. Sun, Y. Zou, Y. Liu, L. Huang, Two nanoformulations induce reactive oxygen species and immunogenetic cell death for synergistic chemo-immunotherapy eradicating colorectal cancer and hepatocellular carcinoma, Mol. Cancer Res. 20 (1) (2021) 1–17, https://doi.org/10.1186/s12943-020-01297-0.
[36] P.S. Mirzaghavami, S. Khoei, S. Khoee, S. Shirvalilou, S.R. Mahdavi, V. P. Mahabadi, Radio-sensitivity enhancement in HT29 cells through magnetic hyperthermia in combination with targeted nano-carrier of 5-Flourouracil, Mater. Sci. Eng. C 124 (2021), 112043, https://doi.org/10.1016/j.msec.2021.112043.
[37] B.A. Ma, C.Y. Sun, Tumor pH-triggered "charge conversion" nanocarriers with on-demand drug release for precise cancer therapy, J. Mater. Chem. B 8 (40) (2020) 9351–9361, https://doi.org/10.1039/D0TB01692F.
[38] X. Gu, C. Shen, H. Li, E.M. Goldys, W. Deng, X-ray induced photodynamic therapy (PDT) with a mitochondria-targeted liposome delivery system, J. Nanobiotechnol. 18 (1) (2020) 87, https://doi.org/10.1186/s12951-020-00644-z.
[39] H.K. Matthews, C. Bertoli, R.A.M. de Bruin, Cell cycle control in cancer, Nat. Rev. Mol. Cell Biol. 23 (1) (2022) 74–88, https://doi.org/10.1038/s41580-021-00404-3.
[40] E. Rozengurt, Autocrine loops, signal transduction, and cell cycle abnormalities in the molecular biology of lung cancer, Curr. Opin. Oncol. 11 (2) (1999) 116–122.
[41] C. Liu, J. Nie, R.S. Wang, W.D. Mao, The cell cycle G2/M block is an indicator of cellular radiosensitivity, 1559325819891008, Dose-Response 17 (4) (2019), https://doi.org/10.1177/1559325819891008.
[42] H. Zhao, Y.F. Zhuang, R.B. Li, Y.Y. Liu, Z.J. Mei, Z.S. He, F.X. Zhou, Y.F. Zhou, Effects of different doses of X-ray irradiation on cell apoptosis, cell cycle, DNA damage repair and glycolysis in HeLa cells, Oncol. Lett. 17 (1) (2019) 42–54, https://doi.org/10.3892/ol.2018.9566.